Simulation and experimental validation of hydraulic collecting in deep-ocean mining

***Guocheng Zhao[1,2], †Longfei Xiao[1,2], Weijie Zhao[1], and Yangrui Cheng[3]**

[1]State Key Laboratory of Ocean Engineering, Shanghai Jiao Tong University, China
[2]Collaborative Innovation Center for Advanced Ship and Deep-Sea Exploration, China
[3]State Key Laboratory of Exploitation and Utilization of Deepsea Mineral Resources, China

*Presenting author: guocheng.zhao@sjtu.edu.cn
†Corresponding author: xiaolf@sjtu.edu.cn

Abstract

Mineral-collecting technology is the core technology of deep-ocean mining, which has a decisive influence on the feasibility and profitability of technology application. Hydraulic collecting method is considered as one of the most promising options to collect the ores in deep-ocean mining system. Therefore, the characteristics of flow field and suction force of single spherical ore particle in the hydraulic collecting was investigated, which have a significant effect on collecting efficiency.

The flow around a spherical manganese nodule placed under a collecting tube was investigated by using Detached Eddy Simulation (DES) and Large Eddy Simulation (LES) based on Shear Stress Transport (SST) model, respectively. A collecting test system was constructed in the laboratory and a series of 285 tests with various working parameter combinations were conducted. The sphere remains still during collecting and the vertical suction force was measured by a force transducer which is connected to the sphere and able to catch the vertical force with high precision. It is verified that the vertical force prediction for single ore particle in collecting condition by simulation with DES/LES method based on SST model is feasible and sufficiently precise, by comparing the results of numerical simulation and tests.

An insight into understanding the characteristics of flow field in hydraulic collecting for deep-ocean mining was provided by comprehensive analysis on dynamic change regularity of wake vortex structures and pressure distribution. The drag coefficients of the sphere with various working parameters were calculated based on test results and defined as approximate equation using dimensionless quantities.

Simulation and experimental validation of spiral flow collecting were also conducted and the values of vertical suction force were measured and compared to that of ordinary flow collecting. The study reveals that the value of vertical force of the sphere in spiral flow is greater than that in ordinary flow under the same test condition. One reason for that is the spiral flow brings about an increase of the transfer distance of low pressure. The results of this study can provide reference and support for mechanism study and optimal design of the hydraulic collecting system for deep-ocean mining.

Keywords: deep-ocean mining, hydraulic collecting, spiral flow, vertical force, simulation, experimental validation

Introduction

The world's growing economy demands more mineral extracted from the ocean. This demand requires the development of the deep-ocean mining technology. Polymetallic nodules are deposited over the ocean floor at water depth of 4,000～6,000 m. They are mostly spherical or ellipsoidal, with their long-axis length varying from 2 cm to 10 cm and a density of 2,100

(Liu et al., 2014)[1]. However, a profitable exploitation of deep-ocean mining is feasible on the premise that there is a nodule collector with maximum collecting capacity of 140 kg of wet nodules per second (Herrouin et al., 1989)[2]. As a result, effective collecting of manganese nodules out of sediment upper layer of deep seafloor is not only one of the key processes of the deep-ocean mining technology, but also the beginning of an economic and environmentally acceptable mining operation.

To pick up these nodules, a variety of collecting methods such as hydraulic methods, mechanical methods and hybrid collection methods have been developed. Commercial production must achieve high sweep efficiency (Chung, 1985)[3]. A sea test (the OMI Test, 1978) showed that hydraulic methods had a higher collecting efficiency than mechanical methods. It is also found that the hydraulic methods have better adaptability to the variation of seabed height than other methods (Zhao et al., 1995)[4].

In the process of hydraulic methods, polymetallic nodules are collected due to the force induced by local high-velocity flow. A number of established computational and experimental results about these methods are available. Hong et al. (1999) dealt with experimental approaches for enhanced understanding of the hydraulic performance of a hybrid pick-up device[5]. The experiments were conducted in a 2-D flume tank. By parametric experiments they found position and shape of baffle plates are significant factors for effective design of hydraulic nodule lifter. Yang et al. (2003) discussed major parameters and their influence on the performance of the pick-up device by tests[6]. The results showed the hydraulic pick-up device with proper dimension and parameters could get high pick-up rate and low content sediments. Chen and Jian (1996) carried out an experimental study on hybrid collection methods[7]. The results showed the relationship between the pick-up efficiency and other key factors.

The flow field of hydraulic collecting for deep-ocean mining is unique and worth of study. Lim et al. (2015) analyzed flow field characteristics with outflow discharge from a collecting device in deep seawater by FLUENT[8]. He revealed seawater velocity and streamline distributions along with complicated flow characteristics downstream including nodule particles behavior.

In contrast to the research about hydraulic collecting, much more studies on the flow around a sphere in a uniform flow field have been done. Achenbach (1972) had experiments on the flow past spheres in the Reynolds number range $5\times104 \leq Re \leq 6\times104$[9]. He compared his results with other available data and pointed out the dependence of friction forces on Reynolds number. Tsutsui (2008) had an experimental study of the flow field and the aerodynamic force on a sphere above a plane[10]. The surface pressures on the sphere and the plane were measured by inclined multi-tube manometers and the results were compared with photographs showing the flow visualization of the sphere.

Johnson and Patel (1999) investigated the flow of an incompressible viscous fluid past a sphere at different Reynolds numbers by DES (Detached Eddy Simulation)[11]. They calculated the instantaneous and mean flow field around the sphere as well as the wake vortex, and validated their numerical results by flow-visualization experiments. On the basis of their analysis, a mechanism driving the transition to unsteady flow was proposed. In the study of Constantinescu and Squires (2003), LES (Large Eddy Simulation) and DES were applied to predict and investigate the flow around a sphere at a Reynolds number of 10,000 in the subcritical regime[12]. Comparison of the computed results with experimental data showed that LES and DES were able to simulate the flow around a sphere.

A number of analyses on hydraulic lifting have also been attempted. Chung et al. (1998) conducted experimental investigation to study the shape effect of solids on pressure drop in a 2-phase vertically upward transport[13]. Their research showed that the spherical particles required a larger $V_{\min}/V_{\mathrm{T}}$ ratio. An experimental investigation about the effects of particle sizes and concentration on pressure gradient or drag was conducted by Chung et al. (2001)[14]. They found that contrary to the conventional perception, 80-100 mesh (0.18-0.15 mm) sands had smaller drag and pressure gradient at enough high Reynolds numbers, as compared to the larger 8-10 (2.36-2.00 mm) and 30-40 (0.6-0.425 mm) mesh sands.

In this study, the flow around a sphere placed at various heights below the bottom of collecting tube was investigated by using DES based on the SST model. Meanwhile, the test system has been constructed in the laboratory and a series of 285 tests with various working parameter combinations were conducted. The vertical force of the sphere was measured and compared with the simulation results. The drag coefficients of the sphere with various working parameters were calculated based on test results and defined as approximate equation using dimensionless quantities. A type of collecting tube with spiral deflectors installed inside was designed, with which spiral flow collecting tests were conducted and the values of vertical suction force were measured and compared to that of ordinary flow collecting.

Numerical Method

In hydraulic collecting, polymetallic nodules will be separated from the sea floor and sucked into the collector when fluidic force overweighs their own gravity and viscous force of sea mud. The schematic diagram is shown in Fig. 1. Unlike the moving equipment in the sea, the collecting tube in our experiments is still.

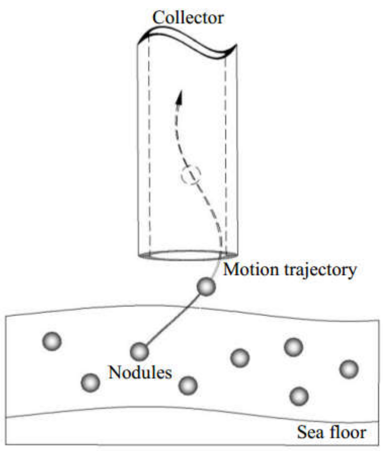

Figure 1. Schematic diagram of hydraulic collecting methods

Computational Domain and Boundary Conditions

According to the physical environment of hydraulic collecting, the computational domain and boundary conditions can be set as shown in Fig. 2 (a)~(b). The collecting height h is the distance between the bottom of the collecting tube and the bottom of the sphere. To simplify the simulation, the sphere is fixed on the bottom of the domain. For flow field analysis, the diameter of the sphere is chosen as d=40mm, which is the typical long-axis length of manganese nodules, and the diameter of the collecting. As for the computational domain, the diameter is 25d, and the height is 7.5d. The impact of the boundary condition on the flow field below the collecting tube can be neglected because the size of the computational domain is sufficiently large.

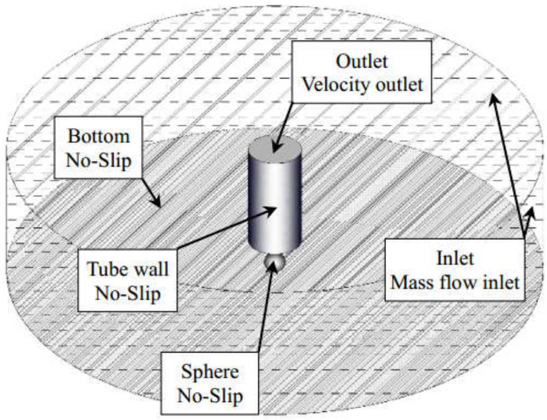

(a) Computational domain and boundary conditions for analysis

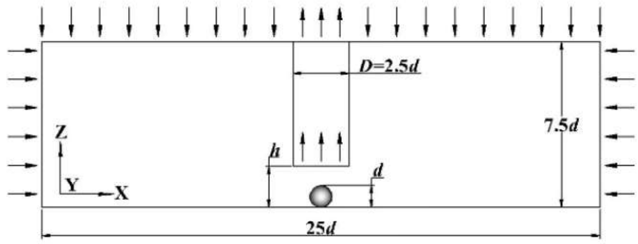

(b) Cutaway view of the computational domain

Figure 2. Computational domain and boundary conditions

Equations of SST Model

The SST-DES is a hybrid RANS/LES model which employs Reynolds-Averaged Navies-Stokes (RANS) in the regions near boundary layers and Large-Eddy Simulation (LES) in the separated region. And the closure model in DES is based on a modification to the Spalart-Allmarars(S-A) one-equation model[15]. When the flow field is simulated by DES, better simulation accuracy can be obtained with less mesh number.

The two equations of Shear-Stress Transport-model (SST model) can be presented as:

$$\frac{\partial(\rho k)}{\partial t}+u_i\frac{\partial(\rho k)}{\partial x_i}=P_k-\frac{\rho k^{\frac{3}{2}}}{l_{k-\omega}}+\frac{\partial}{\partial x_i}\left[\left(\mu_l+\frac{\mu_t}{\sigma_k}\right)\frac{\partial k}{\partial x_i}\right] \tag{1}$$

$$\begin{aligned}\frac{\partial(\rho\omega)}{\partial t}+u_i\frac{\partial(\rho\omega)}{\partial x_i}&=C_\omega P_\omega-\beta_\omega\rho\omega^2+\frac{\partial}{\partial x_i}\left[\left(\mu_l+\frac{\mu_t}{\sigma_k}\right)\frac{\partial k}{\partial x_i}\right]\\&+2\rho(1-F_1)\frac{1}{\sigma_{\omega_2}}\frac{1}{\omega}\frac{\partial k}{\partial x_i}\frac{\partial\omega}{\partial x_i}\end{aligned} \tag{2}$$

and the eddy viscosity is given by

$$\mu_t = \min\left[\frac{\rho k}{\omega}, \frac{a_1 \rho k}{\Omega F_2}\right] \tag{3}$$

where P_k and P_ω are induced by turbulence and are constant in model equations according to the results in Menter (1993)[16].

In the dissipation term of k equation of SST model, the parameter of turbulence scale $l_{k-\omega}$ can be obtained by

$$l_{k-\omega} = k^{1/2} / \beta_k \omega \tag{4}$$

The parameter $l_{k-\omega}$ is replaced by $\min(l_{k-\omega}, C_{DES}\Delta)$ in DES method, where $\Delta = \max(\Delta x, \Delta y, \Delta z)$ is the longest side length of the mesh and C_{DES} is equal to 0.65. In the regions near boundary layers, where $l_{k-\omega}$ is less than or equal to Δ, the DES model can be viewed as SST model. In the separated region, where $l_{k-\omega}$ becomes greater than C_{DES}, the DES model can be considered as LES model.

Experimental Program

Experimental Setup

In order to provide some corroborating evidence for the simulation results, the experimental system is set up to measure the vertical force. Fig. 3 and Fig. 4 show the experimental setup. The water tank used for the experiments was 2.5m long, 1.5m wide and 1.0m deep. Fresh water was sucked from the tank by a pump to simulate the fluid field near the collecting tube. And a frequency transformer was used to give exact adjustments to the rate of the flow through the pump. Precise control of the distance between the bottom of the collecting tube and the center of the sphere was performed by using an ER50-C10 6-dof industrial robot.

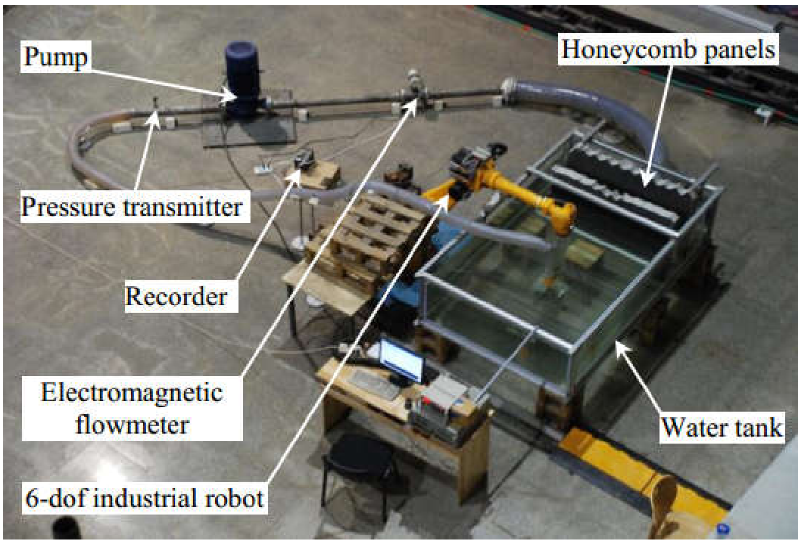

Figure 3. Overall experimental setup

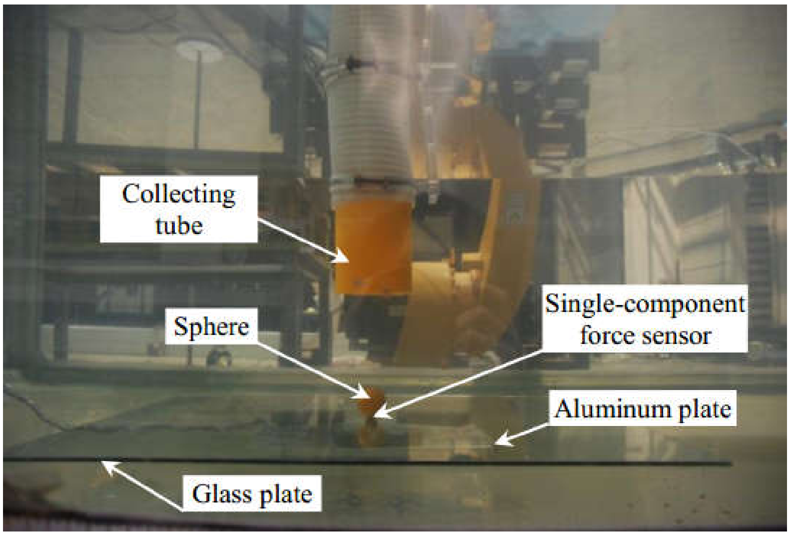

Figure 4. Details of the water tank

The creep and measurement error could be contained within 2‰ by using a LTR-S-5NSA16 single-component force sensor, which meets the requirement of the test. The sensor was fixed on an aluminum plate at the bottom of the water tank. In order to prevent the influence of variation of flow field on the accuracy of sensor measurement, a piece of square glass with the side length of 0.3m and a 7 mm-diameter hole in the center was placed between the sensor and the sphere. Therefore, the sensor was separated from the dynamic fluid flow.

Test Cases

Collecting tubes with different diameters (D=75mm, 100mm, 125mm) were tested under conditions of different collecting heights (varied from 0.050m to 0.080m). In each condition, several sphere sizes were chosen (d=32mm, 36mm, 40mm) and the vertical force exerted on the sphere was measured respectively under different flow velocities of 1.0m/s, 1.2m/s, 1.4m/s, 1.6m/s, 1.8m/s and 2.0m/s. These velocities were chosen to include conditions that hydraulic force on the sphere is smaller or bigger than F_0 (F_0 is equal to the sphere's gravity minus its buoyancy). In order to calculate the critical vertical start force on nodules of identical size, the densities of water and sphere were selected as 1,000 kg/m^3 and 2,100 kg/m^3 (the typical density of manganese nodules on the seabed) respectively. For example, F_0 is 0.3616 N when d=40mm.

For the collecting velocity from 1.0=m/s to 2.0m/s, the Reynolds number based on d (diameter of the sphere) is from around 30,000 to 60,000 when d=40mm. The Re range in actual flow of engineering operation involves some specific collecting conditions such as collecting heights, structures of the collector and local flow velocity of the nodules. There is some possible overlap between our Re range and the actual Re range.

Results and Discussion

Vertical Force

The time-history curves and mean values of vertical force at collecting velocity of 1m/s and 2m/s are shown in Fig. 5. The mean values of numerical results match well with those of experimental measurements.

The oscillation amplitudes of experimental measurements are much larger than those of numerical results, probably because there is some interference in the experiment process such as fluctuations of the free surface, flux changes in the pump and vibration noise.

Due to the periodicity and symmetry of the interference, errors can be offset and accurate mean values can be obtained if we measure for a long time and get enough data. The transverse force also makes a difference on the measurements, but the magnitude of the transverse force is relatively small compared to the vertical force. Therefore, its influence on the transducer can be ignored.

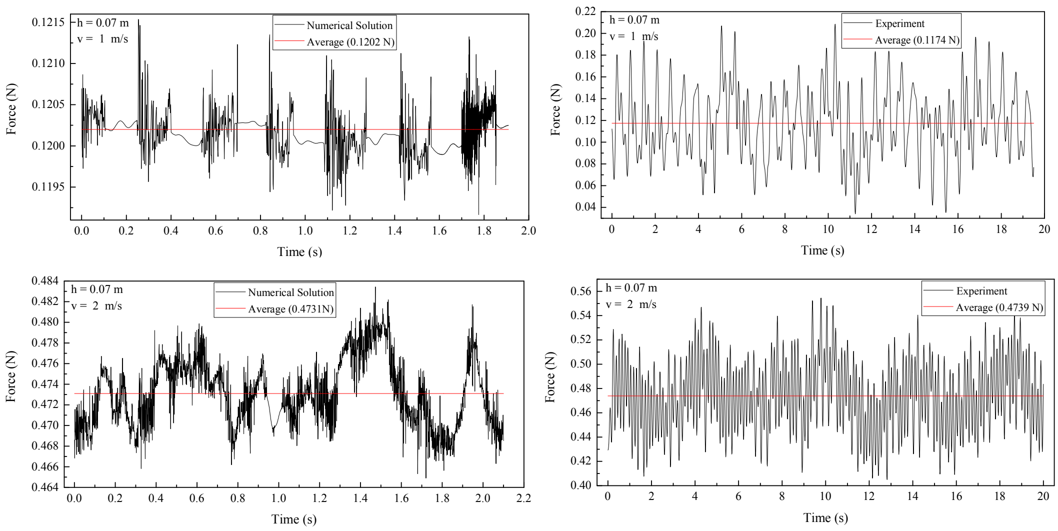

Figure 5. Time-history curves and mean values of vertical force of numerical results and experimental measurements at collecting velocity of 1m/s and 2m/s

(*D*=100mm, *d*=40mm, *h*=0.07m)

Fig. 6 shows the mean values of force on the sphere at different collecting heights and collecting velocities. The overall qualitative behaviors of numerical simulated results and experimental results are in good agreement with each other. Among all the cases, the max difference between test result and CFD result is 5.85%. The comparison validates the feasibility and high accuracy of forecasting the characteristics of the force on an ore particle collected on the seafloor by numerical method. Meanwhile, accurate vertical force measurement can be obtained by the experimental system, which provides a feasible solution for experiments of the special flow around a sphere.

As the collecting height gets smaller, results of the experiments are less than those of the numerical solutions. The arrangement of the sensor may be the cause of the phenomenon. The flow velocity below the sphere would increase when the collecting tube gets closer to the sphere. This would enhance the impact of the sensor placed under the sphere on the experimental measurements. The arrangement of the sensor does not only slightly reduce the area of force of the sphere, but also have a little interference on the fluid field at the bottom of the sphere. This explains the differences between two series of results. The interference of the arrangement of the sensor can be decreased by placing the sensor under the glass plate and extending its tip through a small hole at the center of the plate. In this way, the error could be decreased as much as possible.

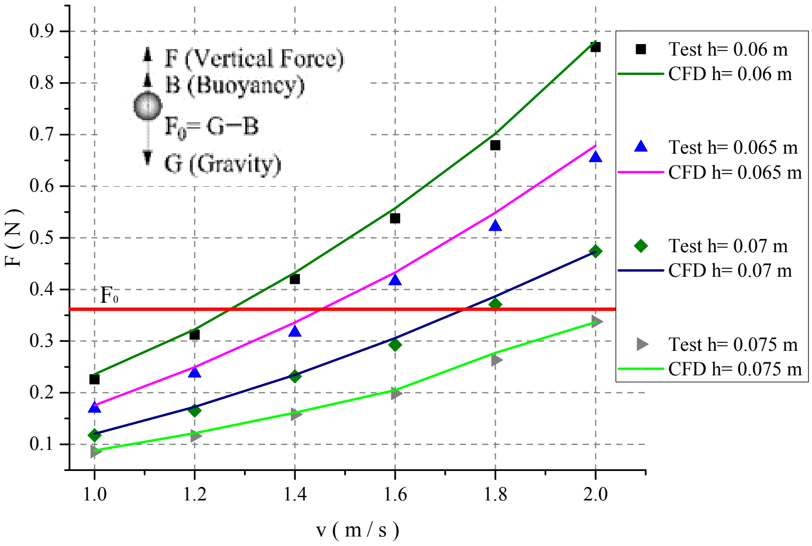

Figure 6. Variation of the mean values of vertical force on the sphere under different collecting heights and collecting velocities (*D*=100mm, *d*=40mm)

Flow Field

The velocity distribution and pressure distribution for collecting height 0.07 m and collecting velocity 2.0m/s are shown in Figs. 7~9. In the collecting flow field, the velocities are relatively larger and the streamlines are more chaotic above the sphere than those velocities and streamlines in other regions, which leads to the forming of turbulent areas in the wake vortex and low pressure areas upon the sphere. Vertical force is induced with the pressure differences along the sphere.

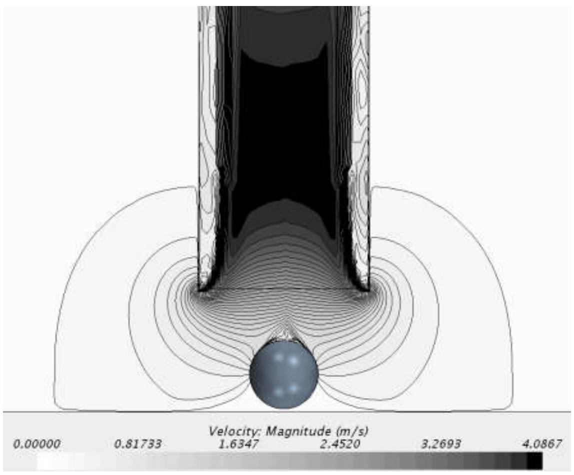

Figure 7. Velocity distribution (*D*=100mm, *d*=40mm, *h*=0.07m, *v*=2.0m/s)

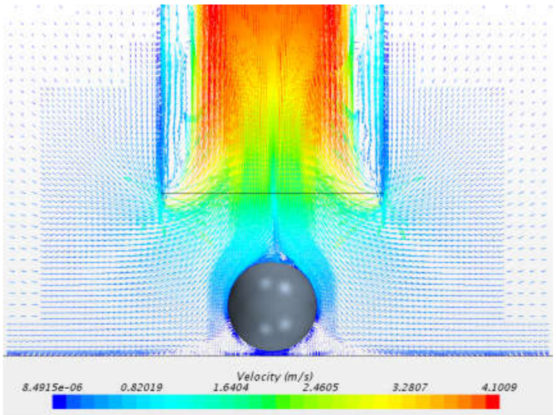

Figure 8. Velocity vector (*D*=100mm, *d*=40mm, *h*=0.07m, *v*=2.0m/s)

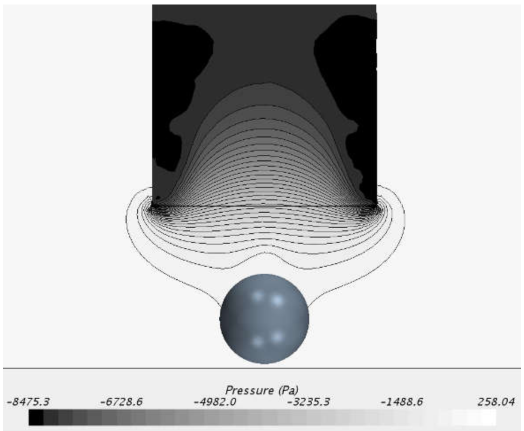

Figure 9. Pressure distribution (*D*=100mm, *d*=40mm, *h*=0.07m, *v*=2.0m/s)

An insight into understanding the characteristics of spherical ore particles is provided in Fig. 10 by the comprehensive analysis on the dynamic change regularity of wake vortex structures and the pressure distribution in one circulation. The repeated growth and burst of the wake vortex is the major reason of the amplitude oscillation of the vertical force.

	F_{max}	$F_{max}\rightarrow F_{min}$	F_{min}	$F_{min}\rightarrow F_{max}$	F_{max}
Pressure distribution	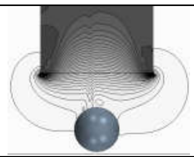	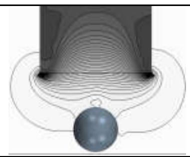	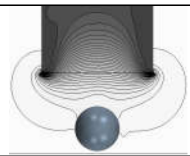	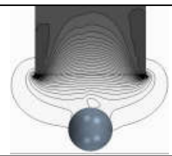	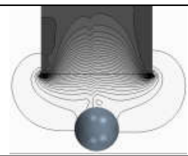
Vortex structure	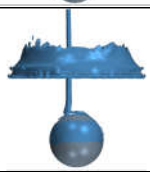			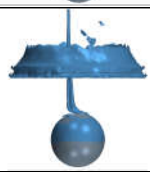	

Figure 10. Development of the pressure distribution and vortex structures

Dimensionless Analysis

Dimensional analysis is applied to find the correlation between the force on the sphere and other experiment data. It is helpful to apply dimensional analysis to analyze the correlation among different parameters in experiment and thus to indicate the cause and effect among them. We can also find out the significance of different parameters with the help of dimensional analysis so as to make it clear what factor plays a key role in the problem. Therefore, it is conducive to deep research of the problem.

In order to discuss the drag coefficient at high Reynolds number, dimensionless quantity C_d is introduced. The physical quantities that determine the drag force are ρ, v, d, μ, D, and h. The dimensionless quantity is obtained by combining these quantities, and C_d is expressed as:

$$C_d = \frac{F}{(1/2)\rho v^2 A} = f\left(\frac{\rho v d}{\mu}, \frac{h}{d}, \frac{D}{d}\right) \tag{5}$$

In addition, we set kinematic coefficient of viscosity as 1.31×10^{-6} $N{\cdot}S/m^2$ in calculations because the water temperature is about 10 degrees Celsius. The relations between drag coefficients and Reynolds numbers, ratios of h/d and D/d were investigated in this paper, based on the results of a series of 285 tests.

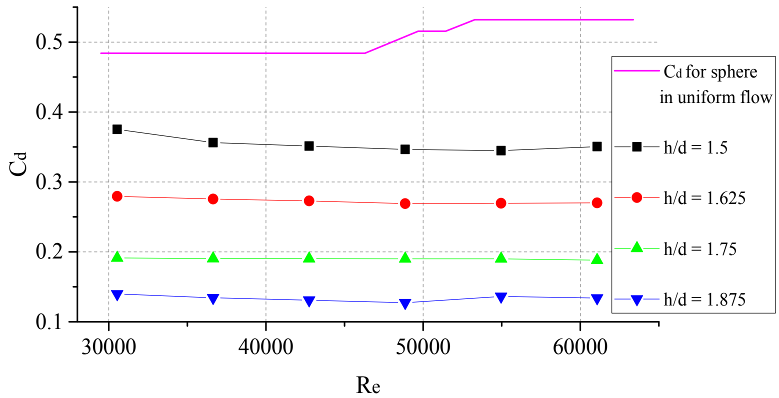

Figure 11. Relations between drag coefficients and Reynolds numbers

(*D*=100mm, *d*=40mm)

As Fig. 11 shows, the drag coefficients for sphere in uniform flow are bigger than those coefficients of our numerical results at the same Reynolds numbers. One reason for this phenomenon is that the pressure gradient changes more violently, another cause is that the detached points of the sphere's wake in the numerical cases are father than that point in uniform flow. Fig. 11 also reveals that the drag coefficients decrease at the same Reynolds number as ratios of h to d grow.

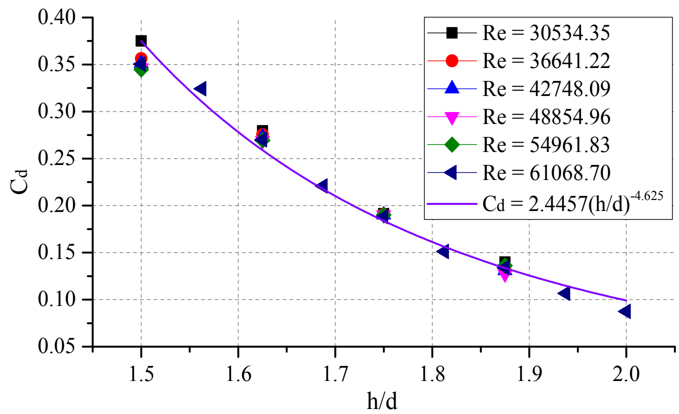

(a) C_d – Re, h/d

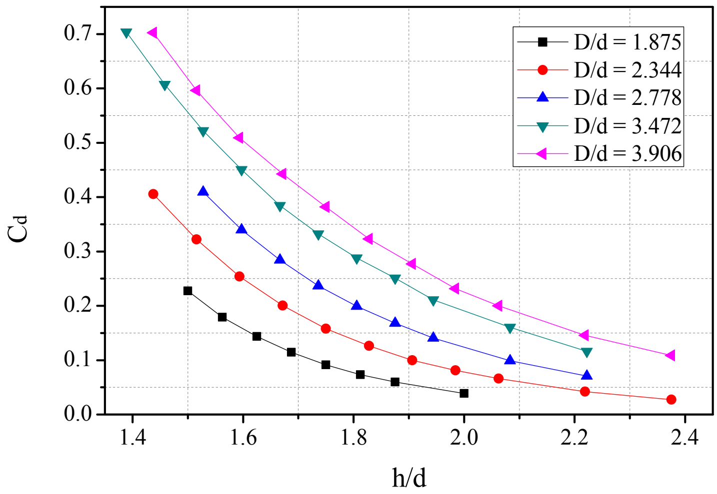

(b) C_d - h/d, D/d

Figure 12. Relations between drag coefficients and Re, *h/d* and *D/d*

As Fig. 12(a) demonstrates, C_d decreases with the increase of h/d in the range of 1.5 to 2.0 but not significantly varies with Re numbers. Fig. 12(b) shows that C_d increases with the increase of D/d when h/d is constant.

The relationship is combined to obtain the following:

$$C_d = 2.8525\left(h/d\right)^{3.3559\left[\ln\left(D/d\right)-2.4084\right]} \tag{6}$$

However, there is no significant relationship between C_d and Reynolds numbers.

Comparison of Vertical Force in Ordinary and Spiral Flow

A type of collecting tube with spiral deflectors installed inside is also designed, which is able to induce spiral flow inside and under the tube. The numerical simulation results of vertical force in ordinary and spiral flow are shown as Table 1 when diameter of the collecting tube D=100mm, tube height above the sphere h=60mm, and diameter of the sphere d=36mm.

Table 1. Vertical force in ordinary flow and spiral flow (*D*=100mm, *h*=60mm, *d*=36mm)

Flow velocity v (m/s)	Vertical force F/N	
	Ordinary flow	Spiral flow
1.0	0.1385	0.1543
1.2	0.2053	0.2223
1.4	0.2834	0.3070
1.6	0.3803	0.4142
1.8	0.4753	0.5228
2.0	0.5849	0.6349

It can be concluded that spiral flow exerts stronger suction force on the sphere as the value of vertical force in the collecting tube with spiral deflectors is much greater. One reason for that is the spiral flow brings about an increase of the scale of vortex structure as is shown in Fig.13.

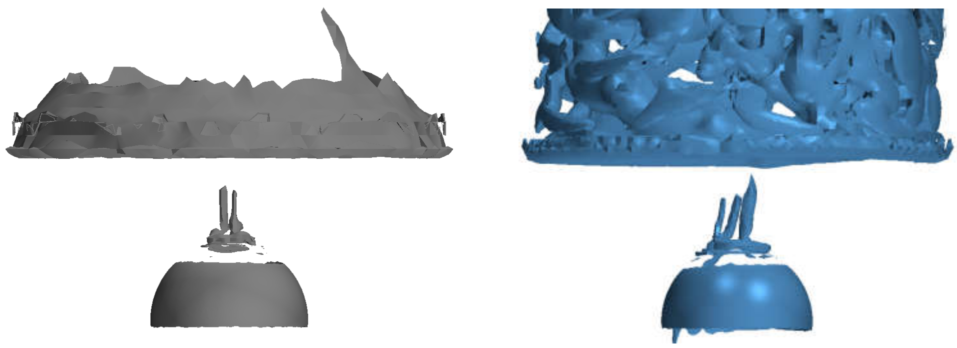

(a) ordinary flow (b) spiral flow

Figure 13. Comparison of the scale of vortex structure

(*D*=100mm, *h*=60mm, *d*=36mm, *v*=1.0m/s)

As to recognizing the vortex structure, Q criteria was applied, where Q is defined as

$$Q = -\frac{1}{2}\left(\|\mathbf{S}\|^2 - \|\mathbf{\Omega}\|^2\right)$$

$\mathbf{S}$, $\mathbf{\Omega}$ represent strain tensor and rotation tensor respectively. In this case Q was chosen as equal to 5000. Fig. 13 indicates that under that condition the scale of wake vortex structure in spiral flow is significantly larger than that in ordinary flow. It means that the scale of low pressure area in the wake flow of the sphere is greater. Therefore, the differential pressure is much larger and the suction force induced by spiral flow is supposed to be much stronger compared to the ordinary flow.

In order to validate the results, model tests with the ordinary collecting tube and the tube with spiral deflectors were conducted and the suction forces were measured respectively. The relations between vertical suction force F and tube height h and flow velocity v in ordinary and spiral flow collecting are shown as Fig. 14, based on test results.

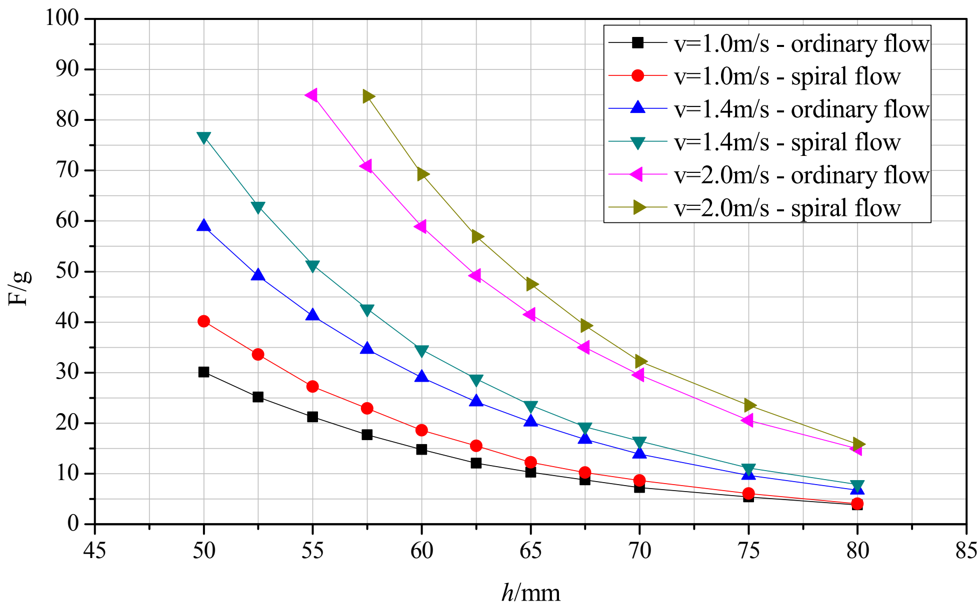

Figure 14. Relations between suction force and tube height and flow velocity in ordinary and spiral flow collecting (*D*=100mm, *d*=36mm)

From Fig. 14 it can be indicated that F increases with the decrease of h, more significantly when h is smaller. Also, it suggests that the suction force of spiral flow is larger than that of ordinary flow at equal flow velocity or flow rate. The ratio reaches about 1.3 at h=50mm according to experiment results.

Conclusions

The flow around a sphere was simulated with detached-eddy simulation (DES) method based on shear stress transport (SST) model, and the wake flow behind the spheres was investigated. Meanwhile, the test system for hydraulic collecting, which is corresponding to the model of CFD, has been set up in the laboratory. A series of 285 tests with various working parameter combinations were conducted. The vertical force of spherical particles is measured by the force transducer. Tests of spiral flow collecting were also conducted and the vertical force results were compared to that of ordinary flow. The following are the main conclusions from this work:

1. The vertical force prediction for single ore particle in collecting condition based on numerical simulation with DES method based on SST model is feasible and sufficiently precise. Also the test system layout is reasonable to be able to catch vertical force with high precision. Therefore, it is a promising method to design the new collector by numerical simulation and test more complex collector by the test system.

2. When h/d is in the range of 1.5 to 2.0 and D/d in the range of 1.875 to 3.906, C_d can be concluded as following:

$$C_d = 2.8525\left(h/d\right)^{3.3559\left[\ln\left(D/d\right)-2.4084\right]}$$

And the drag coefficients for sphere in uniform flow are bigger than those coefficients of our numerical results at the same Reynolds numbers due to different changes of the pressure gradient and the delay of the detached point of the sphere’s wake.

3. The pressure distribution pattern has a significant influence on the vertical force of the sphere. The variation of the wake vortex is the dominant factor of force vibration.

4. The value of vertical suction force of spiral flow is greater than that of ordinary flow at equal flow velocity. Spiral flow brings about an increase of the scale of wake vortex. Therefore, the scale of low pressure area in the wake flow of the sphere is much larger, which forms larger differential pressure and induces stronger suction force on the sphere compared to the ordinary flow.

The results of this study can provide reference and support for mechanism study and optimal design of the hydraulic collecting system for deep-ocean mining. In future research, more working parameter combinations are expected to be designed so as to improve and verify the non-dimensional equation. And the behaviors of the flow and vortices will be observed during flow visualization.

References

[1] Liu, S., Liu, C., and Dai, Y., (2014). “Status and Progress on Researches and Developments of Deep Ocean Mining Equipments,” Journal of Mechanical Engineering, Vol 50, No 2, pp 8-18.

[2] Herrouin, G, Lenoble, JP, Charles, C, Mauviel, F, Bernard, J, .and Taine, B (1989). "A Manganese Nodule

Industrial Venture Would Be Profitable: Summary' of a 4-Year Study in France", Proceedings of Offshore Technology Conference.
[3] Chung, J. S. (1985). “Advances in manganese nodule mining technology.” Marine Technology Society Journal, Vol 19, No 4, pp 39-44.
[4] Zhao, S., and Liu, F., (1995) “Study of Deep-sea Mining Technique In Germany.” Metal mine, No 6, pp 14-17.
[5] Hong, S., Choi, J. S., Kim, J. H., & Yang, C. K. (1999). Experimental study on hydraulic performance of hybrid pick-up device of manganese nodule collector. In The Third ISOPE Ocean Mining Symposium. International Society of Offshore and Polar Engineers. Goa, India, pp 69-77.
[6] Yang, N., & Tang, H. (2003). “Several considerations of the design of the hydraulic pick-up device.” In The Fifth ISOPE Ocean Mining Symposium. International Society of Offshore and Polar Engineers. Tsukuba, Japan, pp 119-122.
[7] Chen, X., and Jian, Q., (1996). “An Experimental Study On Hybrid Collection Method For Deep-sea Nodule Mining.” Mine R & D, Vol 16, No 4, pp 1-4.
[8] Lim, S. J., Kim, J. W., Jung, S. T., Cho, H. Y., and Lee, S. H. (2015). “Deep Seawater flow Characteristics Around the Manganese Nodule Collecting Device.” Procedia Engineering, Vol 116, pp 544-551.
[9] Achenbach, E. (1972). “Experiments on the flow past spheres at very high Reynolds numbers.” Fluid Mech, Vol 54, No 3, pp 565-575.
[10] Tsutsui, T. (2008). “Flow around a sphere in a plane turbulent boundary layer.” Journal of Wind Engineering and Industrial Aerodynamics, Vol 96, No 6, pp 779-792.
[11] Johnson, T. A., and Patel, V. C. (1999). “Flow past a sphere up to a Reynolds number of 300.” Journal of Fluid Mechanics, Vol 378, pp 19-70.
[12] Constantinescu, G. S., and Squires, K. D. (2003). “LES and DES investigations of turbulent flow over a sphere at Re= 10,000.” Flow, Turbulence and Combustion, Vol 70, No 1-4, pp 267-298.
[13] Chung, J. S., Yarim, G., & Savasci, H. (1998). “Shape effect of solids on pressure drop in a 2-phase vertically upward transport: silica sands and spherical beads.” In The Eighth International Offshore and Polar Engineering Conference. International Society of Offshore and Polar Engineers. Montreal, Canada, Vol 1, pp 58-65.
[14] Chung, J. S., Lee, K., Tischler, A., & Yarim, G. (2001). “Effect of particle size and concentration on pressure gradient in two-phase vertically upward transport.” In The Fourth ISOPE Ocean Mining Symposium. International Society of Offshore and Polar Engineers. Szczecin, Poland, pp 132-138.
[15] Spalart, P. R., Jou, W. H., Strelets, M., & Allmaras, S. R. (1997). “Comments on the feasibility of LES for wings, and on a hybrid RANS/LES approach.” Advances in DNS/LES, Vol 1, pp 4-8.
[16] Menter, F. R. (1993). “Zonal two equation k-turbulence models for aerodynamic flows.” AIAA paper, pp 2906.
[17] Hunt, J. C., Wray, A. A., and Moin, P. (1988). “Eddies, streams, and convergence zones in turbulent flows.” Studying Turbulence Using Numerical Simulation Databases, pp 193-208.
[18] Kida, S., Goto, S., and Makihara, T. (2002). “Life, structure, and dynamical role of vortical motion in turbulence.” National Institute for Fusion Science, Theory and Computer Simulation Center, pp 1-2
[19] Ting, L., and Klein, R. (1991). “Viscous vortical flows.” Viscous Vortical Flows, Vol 374.